THYROID
Volume 24, Number 2, 2014

DOI: 10.1089/thy.2013.0127

A Redundant Role of Human Thyroid Peroxidase Propeptide for Cellular, Enzymatic, and Immunological Activity

Marlena Godlewska,[1,*] Monika Góra,[2,*] Ashley M. Buckle,[3] Benjamin T. Porebski,[3] E. Helen Kemp,[4] Brian J. Sutton,[5] Barbara Czarnocka,[1,†] and J. Paul Banga[6,†]

Background: Thyroid peroxidase (TPO) is a dimeric membrane-bound enzyme of thyroid follicular cells, responsible for thyroid hormone biosynthesis. TPO is also a common target antigen in autoimmune thyroid disease (AITD). With two active sites, TPO is an unusual enzyme, and thus there is much interest in understanding its structure and role in AITD. Homology modeling has shown TPO to be composed of different structural modules, as well as a propeptide sequence. During the course of studies to obtain homogeneous preparations of recombinant TPO for structural studies, we investigated the role of the large propeptide sequence in TPO.

Methods: An engineered recombinant human TPO preparation expressed in Chinese hamster ovary (CHO) cells lacking the propeptide (TPOΔpro; amino acid residues 21–108) was characterized and its properties compared to wild-type TPO. Plasma membrane localization was determined by cell surface protein biotinylation, and biochemical studies were performed to evaluate enzymatic activity and the effect of deglycosylation. Immunological investigations using autoantibodies from AITD patients and other epitope-specific antibodies that recognize conformational determinants on TPO were evaluated for binding to TPOΔpro by flow cytometry, immunocytochemistry, and capture enzyme-linked immunosorbent assay. Molecular modeling and dynamics simulation of TPOΔpro comprising a dimer of myeloperoxidase-like domains was performed in order to investigate the impact of propeptide removal and the role of glycosylation.

Results: The TPOΔpro was expressed on the cell surface at comparable levels to wild-type TPO. The TPOΔpro was enzymatically active and recognized by patients' autoantibodies and a panel of epitope-specific antibodies, confirming structural integrity of the two major conformational determinants recognized by autoantibodies. Faithful intracellular trafficking and N-glycosylation of TPOΔpro was also maintained. Molecular modeling and dynamics simulations were consistent with these observations.

Conclusions: Our results point to a redundant role for the propeptide sequence in TPO. The successful expression of TPOΔpro in a membrane-anchored, enzymatically active form that is insensitive to intramolecular proteolysis, and importantly is recognized by patients' autoantibodies, is a key advance for purification of substantial quantities of homogeneous preparation of TPO for crystallization, structural, and immunological studies.

Introduction

Human thyroid peroxidase (TPO) is an oxidoreductase that catalyzes thyroid hormone synthesis at the apical membrane–colloid interface of thyrocytes by iodination of tyrosyl residues of thyroglobulin, and subsequent coupling of iodotyrosyl residues to form the thyroid hormones (1). TPO is also a major antigenic target for autoantibodies in autoimmune thyroid disease (AITD) (2–4).

Polyclonal TPO antibodies present in the sera of patients with AITD react with conformational epitopes restricted to an immunodominant region (IDR) comprising chiefly of two

[1]Department of Biochemistry and Molecular Biology, Medical Center of Postgraduate Education, Warsaw, Poland.
[2]Department of Genetics, Institute of Biochemistry and Biophysics, Polish Academy of Sciences, Warsaw, Poland.
[3]Department of Biochemistry and Molecular Biology, Faculty of Medicine, Monash University, Clayton, Australia.
[4]Department of Human Metabolism, School of Medicine, University of Sheffield, Sheffield, United Kingdom.
[5]Randall Division of Cell & Molecular Biophysics; [6]Division of Diabetes and Nutritional Sciences, School of Medicine; King's College London, London, United Kingdom.
*Joint first authors.
†Joint senior author contribution.

overlapping regions A and B (2–4). These regions were firstly defined in competition experiments with a panel of murine monoclonal antibodies and patient autoantibodies (5), and subsequent studies with recombinant human anti-TPO Fab fragments confirmed these findings (6,7). Numerous attempts have been made to identify the amino acids in the autoantibodies' epitopes (8–18); however, to clearly interpret these data and arbitrate between some conflicting results, the determination of the three-dimensional structure of TPO in complex with various autoantibodies is needed.

The human *TPO* gene on chromosome 2 is comprised of 150 kb, consisting of 17 exons and 16 introns (19). The protein of 933 amino acids has been shown to have a large N-terminal extracellular ectodomain, a single transmembrane region and a short cytoplasmic C-terminal tail. The ectodomain is composed of an N-terminal signal peptide, a propeptide, and three domains: an N-terminal myeloperoxidase (MPO) domain (MPO-like, residues 142–738), a complement control protein domain (CCP-like, residues 739–795), and a C-terminal epidermal growth factor domain (EGF-like, residues 796–841) (9). The signal peptide is encoded by part of exon 2, but the exact physiological cleavage site remains unknown. It has been proposed to occur between residues 14 and 15, 18 and 19, or 26 and 27 (20). The propeptide is encoded by exons 2 to 4, but its functions are unclear (20). Moreover, sequence alignment of TPO from different species indicates a high degree of homology, except for the N- and C-terminal regions (21), but interestingly the propeptide region of TPO in different species shows minimal homology (20).

Newly synthesized TPO is transported from the endoplasmic reticulum to the cell surface via the Golgi complex (20,22–24). During processing and intracellular trafficking TPO interacts with the molecular chaperones calnexin, calreticulin (25), and BiP (26). It also undergoes several posttranslational modifications, notably glycosylation, heme fixation (within the MPO domain), proteolytic trimming, and dimerization. On sodium dodecyl sulfate polyacrylamide gel electrophoresis (SDS-PAGE), the purified TPO migrates as two closely spaced bands of about 100 kDa and despite intensive studies, it has been difficult to resolve whether the two protein bands are derived by proteolytic processing, presence of various mRNA species encoding for different TPO isoforms, or posttranslational modifications (20,27,28). Elegant studies by Le Fourn and colleagues (20) on purified preparations of TPO from human thyroid tissue revealed N-terminal processing to be at the end stage in the endoplasmic secretory pathway. Furthermore, analysis of the effect of removal of the postulated propeptide (Cys15–Lys108) on TPO expression in Chinese hamster ovary (CHO) cells suggested that the propeptide acts as an intramolecular chaperone facilitating proper TPO folding (20). In our studies to obtain homogeneous preparations of the soluble TPO ectodomain for crystallization and structural studies, we focused on enzyme preparations lacking the propeptide sequence that are expressed in CHO cells. We obtained high levels of expression and successfully purified a single species of recombinant TPO lacking the TPO propeptide sequence. Surprisingly, our data indicated that the absence of the propeptide sequence does not appear to influence the folding, trafficking and cell surface expression, incorporation of the heme moiety, enzymatic activity, and binding of conformation-dependent autoantibodies.

Materials and Methods

Antibodies

Recombinant human Fabs (rhFabs) specific for IDR-A (126TP1 and 126TO10) and specific for IDR-B (126TP5 and 126TP14) were obtained and characterized as previously described (6,29). Pooled sera from 20 patients with AITD were obtained from the Regional Hospital Siedlce (Siedlce, Poland). These sera were positive for TPO antibodies and were used as a positive control in flow cytometry and capture enzyme-linked immunosorbent assay (ELISA). A rabbit anti-peptide P14 polyclonal antibody that specifically binds to region 599–614 of TPO was generated and characterized previously (9,10). Murine monoclonal antibody (mAb) A4 directed to a linear epitope on TPO (30) was used in capture ELISA and Western blotting. A murine mAb specific to beta-actin (clone AC-15) from Abcam was used in Western blotting. We use the terminology of IDR-A and -B established by Ruf *et al.* (5).

Construction of cDNA encoding wild-type TPO and TPO lacking the propeptide and their expression in Chinese hamster ovary cells

Cloning of full-length recombinant human *TPO* cDNA was previously described (11). A cDNA coding for *TPO* lacking the propeptide (TPOΔpro) was prepared using an overlap extension polymerase chain reaction (PCR) (31). In the primary PCR amplifications, in which pcDNA5/FRT–wild-type TPO (TPOwt) served as a template, the primers were upstream 5′-CGC AAG CTT GTC AGA ATG AGA GCG CTC GCT-3′ plus downstream 5′-TGG ATG CTG TGA TTG TTG AGT GAA GAA GGC TTC TGT GCA GGC-3′, and upstream 5′-ACT CAA CAA TCA CAG CAT CCA-3′ and downstream 5′-CAC GTA CTG CTG GAA GGC CTC-3′, respectively. The PCR products were isolated from agarose gel and then simultaneously subjected to the secondary PCR with the following primers: upstream 5′-CGC AAG CTT GTC AGA ATG AGA GCG CTC GCT-3′ and downstream 5′-CAC GTA CTG CTG GAA GGC CTC-3′. The final product was digested simultaneously with *Hin*dIII and *Bam*HI and cloned into pcDNA5/FRT vector (Life Technologies) resulting in the construct pcDNA5/FRT/TPO *Hin*dIII-*Bam*HI. Then the *Bam*HI-*Not*I fragment was subcloned from pcDNA5/FRT/TPOe into pcDNA5/FRT/TPO *Hin*dIII-*Bam*HI to generate pcDNA5/FRT/ΔproTPOe. The construction of the pcDNA5/FRT/TPOe vector, which contained the cDNA encoding the extracellular domain of TPO, was conducted previously by subcloning a *Nhe*I-*Not*I fragment from pCIneo/TPOe (10) to pcDNA5FRT. Finally, a *Bam*HI-*Not*I fragment was subcloned from pcDNA5/FRT/TPOwt into pcDNA5/FRT/ΔproTPOe.

Transfection and expression of recombinant TPO in Chinese hamster ovary (CHO) cells using the Flp-In expression system was previously described (11). Cell lines resistant to 600 μg/mL Hygromycin B (Life Technologies) were propagated for stable expression.

Total cell protein isolation and cell surface protein biotinylation

Total cell proteins were extracted from CHO cells as previously described (12). Cell surface protein was isolated using the Cell Surface Protein Isolation Kit (Pierce) according to the protocol provided by the manufacturer. In brief, the cells were grown to 90%–95% confluence and were then rinsed twice

with ice-cold phosphate-buffered saline (PBS) and subsequently incubated for 30 minutes with 0.25 mg/mL Sulfo-NHS-SS-Biotin in PBS at 4°C. After quenching of the remaining reactive Sulfo-NHS-SS-Biotin, the cells were lysed in buffer supplemented with protease inhibitor cocktail Complete (Roche). To isolate surface proteins, NeutrAvidin Agarose beads were added and mixed for 1 hour at room temperature. Biotinylated surface proteins were separated from the intracellular protein fraction by centrifugation. The beads were washed four times with the buffer provided by the manufacturer supplemented with protease inhibitor cocktail Complete (Roche), and the surface proteins were eluted by the addition of SDS-PAGE sample buffer with 50 mM dithiothreitol. The reaction was mixed for 1 hour at room temperature. Actin was used as a control to show that the intracellular proteins were not biotinylated.

Immunodetection of TPO

Proteins extracted from CHO cells were resolved by SDS-PAGE gels under reducing and nonreducing conditions, and electrophoretically transferred to nitrocellulose membranes. The membranes were probed with anti-TPO mAb A4 and anti-beta-actin mAb (Abcam) as primary antibodies, followed by incubation with a horseradish peroxidase (HRP)-conjugated rabbit anti-mouse IgG (Dako), and developed using chemiluminescence SuperSignal West Pico Substrate System (Pierce). The amount of TPO expressed by CHO transfectants was standardized by densitometry.

Immunocytochemistry

Cells grown on uncoated glass coverslips for 3 days were washed with PBS, fixed with 4% paraformaldehyde for 15 minutes, followed by a brief wash in PBS and quenching with 50 mM NH_4Cl in PBS for 10 minutes. The cells on selected coverslips were permeabilized for 5 minutes with 0.1% Triton X-100 in PBS. After three washes in PBS, all preparations were then blocked with 2.5% goat serum and 2.5% bovine serum albumin (BSA) in PBS for 1 hour. For the permeabilization, the blocking and all subsequent incubation and washing steps included 0.1% Tween 20. After brief washing in PBS, the cells were incubated with mAb A4 (0.2 μg/mL) in blocking solution for 1 hour. The cells were washed three times with PBS and incubated with goat anti-mouse IgG DyLight 549-conjugate (Abcam) for 1 hour. The cells were further washed three times with PBS and incubated with 4',6-diamino-2 phenylindole for 5 minutes. The cells were finally washed once in PBS before mounting and visualization with a Zeiss AxioVision microscope equipped with epifluorescence optics, digital camera, and Zeiss AxioVision software. All steps were carried out at room temperature.

Flow cytometry analysis

Cell surface expression of TPOwt and TPOΔpro was analyzed with anti-TPO-specific rhFabs and a pool of 20 sera from patients with AITD positive for autoantibodies to TPO as already described (8). A 48-hour culture of CHO cells was detached from culture plates with nonenzymatic Cell Dissociation Solution (Sigma-Aldrich) and washed with PBS containing 0.1% BSA. The cells were resuspended and incubated for 30 minutes at 4°C with TPO-specific primary antibodies, washed, and incubated for 30 minutes at 4°C with R-phycoerythrin-conjugated anti-human kappa (Caltag) or fluorescein isothiocyanate–conjugated anti-human IgG (Sigma-Aldrich). Then the cells were washed, fixed in 2% formaldehyde in PBS, and evaluated (10,000 events) on a FACSCalibur flow cytometer and analyzed with CellQuest software (Becton Dickinson).

Capture ELISA

For assessing the binding of rhFabs, a pool of 20 sera from patients with AITD and anti-P14 antibody to TPO was studied by capture ELISA as described with some minor modifications (8,11). In brief, the wells of polystyrene high-binding microtiter plates (Costar) were coated with mAb A4 at 30 μg/mL in carbonate-bicarbonate buffer containing 0.1% sodium azide and incubated overnight at 4°C. After each incubation, wells were washed three times with TBS containing 0.1% Tween 20 (TBST). After blocking by incubation with TBS containing 2 mg/mL BSA, total cell proteins extracted from CHO cells were added at 10 μg/mL in TBST containing 2 mg/mL BSA (TBST-BSA). The following day, anti-TPO-specific antibodies were diluted in TBST-BSA to give an OD at 450 nm between 1.0 and 2.0, and incubated 1 hour at room temperature. The bound Fab fragments or patient or rabbit antibodies were detected after incubation for 1 hour at room temperature with a HRP-conjugated goat anti-human IgG Fab-specific (Sigma-Aldrich), a HRP-conjugated rabbit anti-human IgG (Sigma-Aldrich), or a HRP-conjugated goat anti-rabbit IgG (Dako), respectively. The plates were developed with 0.1 mg/mL tetramethylbenzidine (TMB) in citrate buffer, pH 4.0. The reaction was terminated with 100 μL of 1 M sulfuric acid and optical density was measured at 450 nm in a microtiter reader (Multiscan RC, Labsystems).

Deglycosylation with Endo H and PNGase F

Protein samples were denatured by boiling for 10 minutes in 0.5% SDS and 1% 2-mercaptoethanol. Samples were then diluted with the buffer used for incubation with glycosidases. Endo H (Roche) and PNGase F (New England Biolabs) digestion were performed in 50 mM sodium acetate (pH 5.0) or 1% NP-40 in PBS (pH 7.5), respectively. The samples were incubated for about 16 hours at 37°C. Control reactions were performed under the same assay conditions except that the deglycosylation enzymes were omitted. Then the SDS-PAGE sample buffer was added to each reaction.

Enzymatic activity of extracellular TPO

Enzymatic activity of TPO expressed at the surface of the cell was determined as previously described (32) with some minor modifications. CHO cells were grown for 48 hours in six-well plates in a medium supplemented with 20 μM hemin (Sigma-Aldrich). The cells were washed two times with 2 mL of PBS, then 0.5 mL of reaction mixture was added (100 μM KI [Sigma-Aldrich], 200 U/mL SOD [Sigma-Aldrich], and 50 μM Amplex Ultra Red [Life Technologies] in PBS). The reaction was initiated by adding 25 μL of 1 mM H_2O_2 (Sigma-Aldrich). Twenty-microliter aliquots were removed at 1-minute intervals during 8 minutes and immediately mixed with 80 μL of inhibition mixture containing 500 U/mL catalase (Sigma-Aldrich) and 100 U/mL superoxide dismutase (Sigma-Aldrich)

in PBS. The fluorescence was measured in a microtiter reader (Synergy H4, Biotek) using excitation at 530 nm and emission at 590 nm.

Statistical analysis

The statistical significance was determined by the Mann-Whitney *U* test using Statistica 10.0 software (StatSoft, Inc.). The difference was considered significant at $p < 0.05$.

Modeling the MPO-like domain dimer of TPO

A model of the human MPO-like domain from TPO (residues 139–736) was constructed first by querying the protein sequence against the Protein Databank (PDB) using the NCBI BLAST web server (http://blast.ncbi.nlm.nih.gov/Blast.cgi). Searching through the resulting structures led to the selection of bovine lactoperoxidase (LPO; PDB 3Q9K) as a template structure, having a sequence identity of 47% with the MPO-like domain from human TPO. This structure was selected over the other high-identity structures because it features a full contiguous structure, which is similar to the MPO-like domain of TPO. The TPO-MPO sequence was aligned against the 3Q9K sequence using ClustalW (33). Using the PDB structure and sequence alignment, 100 homology models were built using MODELLER (34). The best scoring model was selected for building an MPO-like domain dimer using as a template the structure of human MPO isoform C dimer (PDB 1CXP). The interdimer disulfide bridge (residues 153 in 1CXP) was modeled in the MPO-like domain dimer model.

Molecular dynamics simulation of the MPO-MPO domain dimer model of TPO

The MPO-MPO domain dimer model was placed into a cubical box of 14.6 nm^3 with a minimum distance of 1.4 nm between the protein and the wall of the box. The system was solvated in explicit water followed by the addition of counterions (Na^+ or Cl^-) to a concentration of 50 mM NaCl, thereby neutralizing the net charge of the system. The simulation box was subjected to a steepest descent energy-minimization before commencing dynamics. To avoid unnecessary distortion of the protein during the initial stages of simulation, a gradual positional restraints equilibration was used. Here, three consecutive equilibration runs were performed in which all heavy protein atoms were restrained to their starting positions using a force constant of 1000, 100, and 10 $kJ/mol/nm^2$ respectively. The equilibration stage initially heated the system to 298 K while restraining the heavy protein atoms with a force of 1000 $kJ/mol/nm^2$ for 100 picoseconds. The restraining force was released to 100 $kJ/mol/nm^2$ for 100 picoseconds, followed by the release to 10 $kJ/mol/nm^2$ for another 100 picoseconds.

The equilibrated MPO-MPO domain dimer system was then subjected to a production simulation for 300 nanoseconds, with configurations stored every 10 picoseconds for analysis. Simulations were carried out using GROMACS Ver. 4.0.7 (35) in conjunction with the GROMOS 53A6 united-atom force field (36). Ionizable residues were in their standard protonation states at pH 7.0. Water was explicitly represented using the simple-point-charge model (37). Simulations were performed in an NPT ensemble under periodic boundary conditions. Simulation conditions were roughly the same as described in Oostenbrink *et al.* (36). The temperature was maintained close to its reference value of 298 K by independent weak-coupling of the protein and solvent to an external temperature bath with a coupling constant of $\tau_T = 0.1$ picoseconds (38).

The pressure was maintained close to its reference value of 1 bar by isotropic weak-coupling of the atomic coordinates and box dimensions to a pressure bath (38), using an isothermal compressibility value of 4.6×10^{-5}/bar and a coupling constant of $\tau_P = 1$ picosecond. During the simulations, the bond length within the protein was constrained using the P-LINCS algorithm (39) and water geometry was constrained using the SETTLE algorithm (40). The time step used for integrating the equations of motion was 2 femtoseconds.

Nonbonded interactions were evaluated using a twin-range cutoff scheme: interactions falling within the 0.8 nm

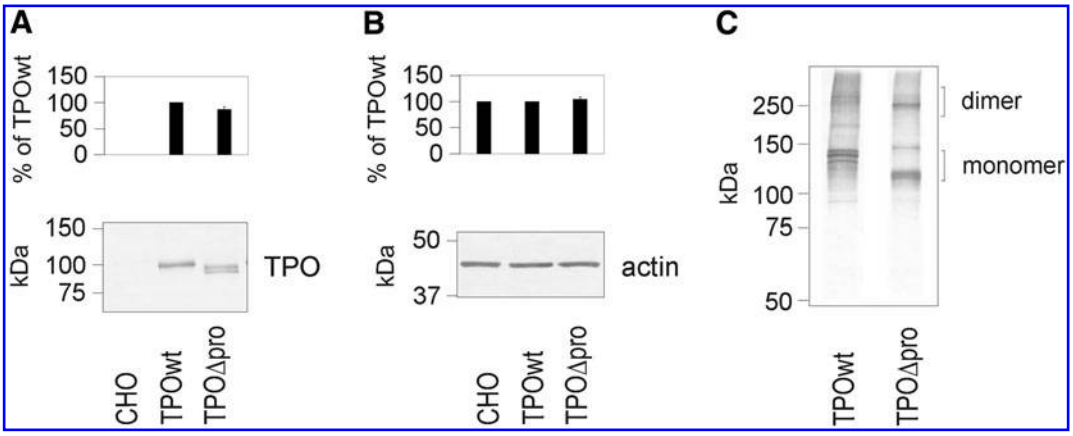

FIG. 1. Western blot analysis of TPOwt and TPOΔpro expressed in CHO cells under **(A, B)** reducing and **(C)** nonreducing conditions. Five micrograms of total cell lysate was loaded onto 8% SDS-PAGE per lane, transferred to nitrocellulose membranes and probed with **(A, C)** anti-TPO mAb A4 and **(B)** anti-beta-actin mAb. One representative immunoblot from independent experiments ($n \geq 3$) is shown. The densitometric quantification (means ± SD) of the bands is shown on the top of panels **(A)** and **(B)**. Non-transfected CHO cells were used as a negative control **(A, B)**. TPO, thyroid peroxidase; wt, wild-type; TPOΔpro, recombinant human TPO preparation lacking the propeptide; CHO, Chinese hamster ovary; SDS-PAGE, sodium dodecyl sulfate polyacrylamide gel electrophoresis; mAb, monoclonal antibody.

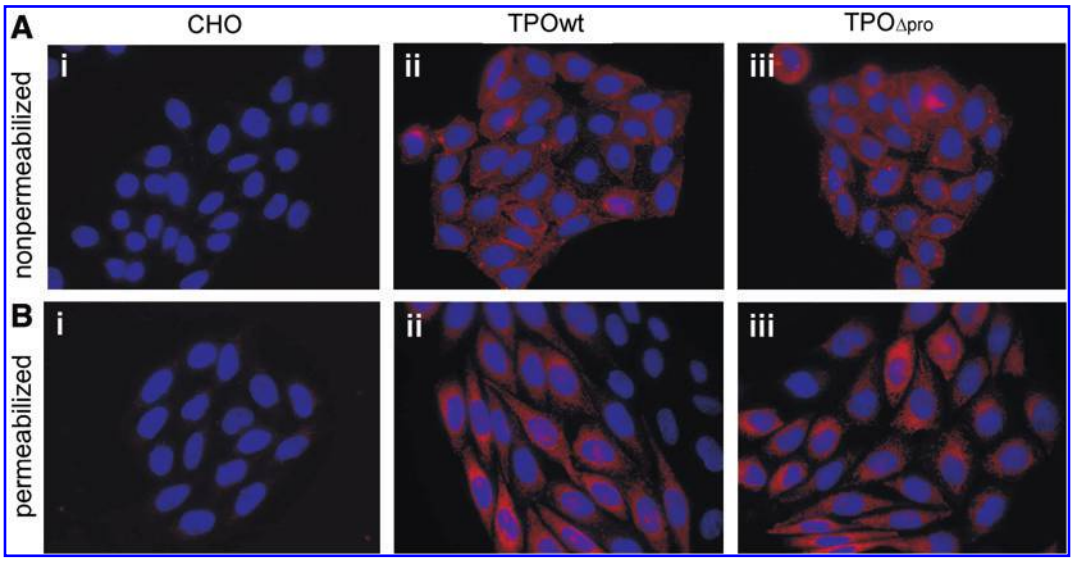

FIG. 2. Immunofluorescence distribution of thyroid peroxidase in stably transfected CHO cells expressing TPOwt **(ii)** and TPOΔpro **(iii)**. Non-transfected CHO cells were used as a negative control **(i)**. Fixed cells were nonpermeabilized **(A)** or permeabilized with 0.1% Triton X-100 **(B)**. TPO was detected using mAb A4 and visualized with goat anti-mouse IgG DyLight 549 (red) conjugate at ×100 magnification. 4′,6-Diamino-2 phenylindole (blue) was applied to visualize nuclei. One representative of three experiments is shown. Color images available online at www.liebertpub.com/thy

short-range cutoff were calculated every 2 femtoseconds, whereas interactions within the 1.4-nm-long cutoff were updated together with the pair list every 10 femtoseconds. A reaction-field correction was applied to the electrostatic interactions beyond the long-range cutoff (41) using a relative dielectric permittivity constant of $\varepsilon_{RF} = 62$ as appropriate for simple-point-charge water (42). The system was simulated three times independently, each time starting with a different distribution of initial velocities.

Results

Construction, expression, and immunoreactivity of TPOwt and TPOΔpro

We constructed a *TPO*-cDNA, called TPOΔpro lacking the sequence encoding Pro21–Lys108, but with an intact signal sequence (residues 1–20) for expression in CHO cells. Full-length TPOwt produced in CHO cells was used as a control. Immunoblotting analysis under reducing conditions of total cell lysates revealed that TPOΔpro is expressed at a similar level as TPOwt (Figs. 1A and 1B). Under nonreducing conditions, we observed the presence of high molecular weight TPO bands in total cell lysates extracted from both TPOwt and TPOΔpro (Fig. 1C).

We then examined the immunofluorescence localization of TPOwt and TPOΔpro in nonpermeabilized (Fig. 2A) and permeabilized CHO cells (Fig. 2B). Thyroid peroxidase was detected with linear epitope-specific antibody mAb A4. Both TPOwt- and TPOΔpro-expressing cell lines, after treatment with Triton X-100, showed strong perinuclear and reticular fluorescence throughout the cytoplasm, suggesting localization in the endoplasmic reticulum. Under

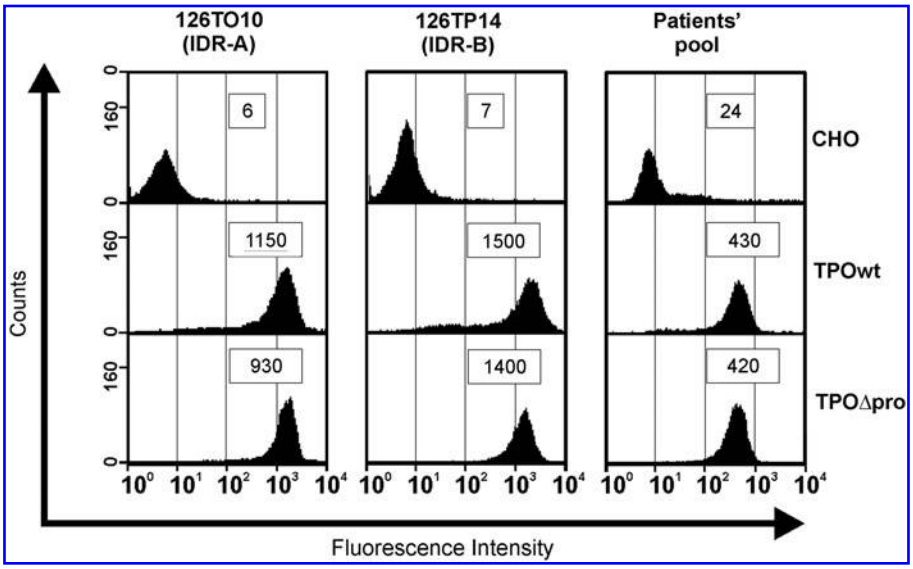

FIG. 3. Flow cytometry analysis of binding of recombinant human Fabs (rhFabs) 126TO10 and 126TP14 (specific for IDR-A and -B, respectively) and a pool of 20 sera from patients with autoimmune thyroid disease (AITD) to TPOwt and TPOΔpro expressed on the surface of stably transfected CHO cells. Non-transfected CHO cells were used as a negative control. Fluorescence was developed as described in **Materials and Methods.** Data are representative of two independent experiments. Mean values of fluorescence are shown in boxes.

nonpermeabilization conditions, the same lines exhibited immunofluorescence that was located at the cell membrane with a punctuate pattern. TPO-specific staining was not observed in a non-transfected CHO cell line used as a negative control (Fig. 2A-i, B-i). These results suggest that the cell distribution of full-length and truncated TPO is comparable.

Flow cytometry and anti-TPO Ab reactivity were used to confirm the cell surface exposure of truncated and wild-type TPO (Fig. 3), as indicated by immunofluorescence. First, we verified that cell lines express TPO at the surface using a human anti-TPO serum pool. We observed a similar positive binding profile between the TPOΔpro and TPOwt cell lines, whereas no binding was observed with the control cells (non-transfected CHO cells). Next, we evaluated the reaction of wild-type and truncated TPO with IDR-A (126TO10)-specific and IDR-B (126TP14)-specific rhFabs (Fig. 3). These results demonstrate that the reactivity of truncated TPO with conformation-dependent antibodies is not substantially affected by removal of the propeptide.

To confirm that the TPOΔpro was immunologically intact we applied capture ELISA tests with mAb A4 (Fig. 4). We showed earlier (8) that this method is more sensitive than flow cytometry in detecting changes in the antibody–antigen reactivity. In this study, we used four rhFabs, two specific for region A (126TO10 and 126TP1) and two specific for region B (126TP5 and 126TP14), polyclonal anti-peptide P14 rabbit serum, interacting with region B (9,10), and a pool of sera collected from patients with AITD. We observed small but statistically significant reductions in the reactivity of truncated TPO with all tested antibodies except for rabbit anti-peptide P14 serum (Fig. 4). In all cases, the decrease in the reactivity was never greater that about 20%.

Extracellular TPO activity

To analyze extracellular TPO activity, we incubated CHO cells expressing truncated and wild-type TPO (positive control) and non-transfected CHO cells (negative control) with sensitive fluorogenic substrate (Amplex Ultra Red, Life Technologies) in the presence of hydrogen peroxide. Accumulation of the fluorescent reaction product was measured in real time. Each well was seeded with the same number of cells to reach 100% confluence on the day of experiment. Cells were grown in the culture medium supplemented with heme precursor (hemin).

We observed similar TPO activity in both TPO-expressing cell lines (Fig. 5), confirming that truncated TPO is effectively transported to the cell surface and acquires full enzymatic activity. To confirm the validity of the method, we conducted additional control experiments, in which CHO cells expressing TPOwt secreted into the culture medium (TPO ectodomain) and thyrotropin receptor (protein bound to the cell membrane) were used (data not shown). Neither control cell lines resulted in peroxidase activity as measured by the oxidation of fluorogenic substrate (activity level similar to that of non-transfected CHO cells).

Analysis of glycosylation

While determining the TPO expression in total cell lysates extracted from CHO cells by immunoblotting (Fig. 1A), we observed, surprisingly, that truncated TPO migrated under

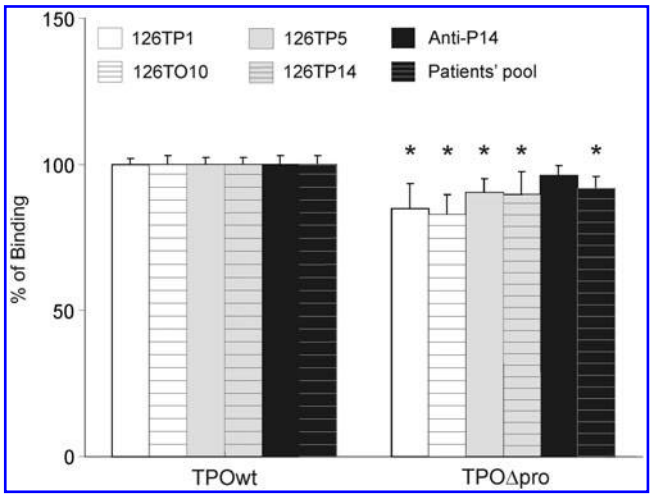

FIG. 4. Relative reactivity of rhFabs specific for IDR-A (126 TP1 and 126TO10) and IDR-B epitopes (126TP5 and 126TP14), rabbit anti-peptide P14 serum (specific for IDR-B), and a pool of 20 sera from patients with AITD to TPOwt and TPOΔpro by capture enzyme-linked immunosorbent assay (ELISA). Total cell lysates from CHO cells were captured onto microtiter plates coated with anti-TPO mAb A4, followed by incubation with the appropriate anti-TPO antibodies. Data are presented as percentage values of TPOwt reactivity (means ± SD). Background binding to membrane proteins prepared from non-transfected CHO cells was subtracted from the antibody binding to proteins extracted from CHO cells expressing TPOwt and TPOΔpro. The results shown are representative of three independent experiments, performed in triplicate wells. The OD values (means ± SD) for TPOwt and TPOΔpro, respectively, from one representative experiment with rhFab 126TO10 are 1.99 ± 0.08 and 1.83 ± 0.02; with rhFab 126TP1, 1.99 ± 0.10 and 1.77 ± 0.04; with rhFab 126TP5, 1.82 ± 0.06 and 1.72 ± 0.04; with rhFab 126TP14, 1.95 ± 0.06 and 1.86 ± 0.02; with rabbit anti-P14 serum, 1.53 ± 0.12 and 1.50 ± 0.01; and with patients' pool, 1.35 ± 0.12 and 1.32 ± 0.01. Asterisks mark statistically significant differences in antibody binding between TPOwt and TPOΔpro determined using the Mann-Whitney *U* test (*$p < 0.05$).

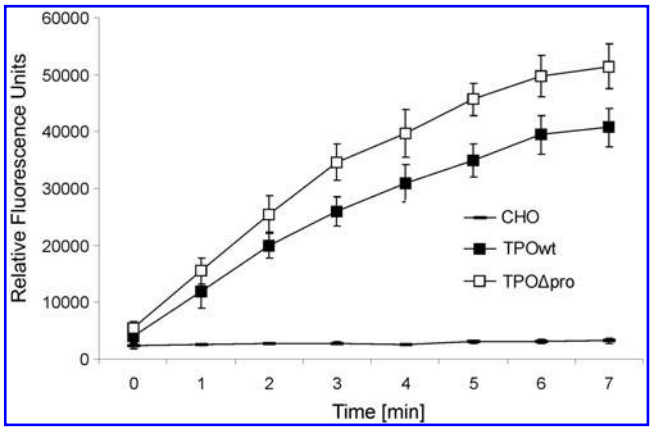

FIG. 5. Extracellular activity of TPO measured by the Amplex Ultra Red (Life Technologies) oxidation of cells expressing TPOwt and TPOΔpro. Non-transfected CHO cells were used as a negative control. Data are presented as relative fluorescence units (means ± SD).

reducing conditions as a double band (104.2 ± 7.3 and 98.0 ± 3.0 kDa), in contrast to a single band observed for TPOwt (107.6 ± 2.6 kDa). We hypothesized that two bands of TPOΔpro may originate from differential N-linked glycosylation. Thus, we incubated total cell lysates with PNGase F in an attempt to remove all asparagine-linked sugar moieties (Fig. 6). After treatment with PNGase F, TPOΔpro migrated on SDS-PAGE gel as a single distinct band (83.4 ± 3.1 kDa) (Fig. 6, lane 4). This strongly suggests that truncated TPO undergoes posttranslational N-glycosylation, acquiring approximately 17 kDa of N-linked carbohydrate. This is consistent with the reported 12 kDa N-linked glycosylation of TPOwt (20). PNGase F-treated TPOwt yielded three bands (99.1 ± 3.6, 94.9 ± 0.1, 92.6 ± 5.2 kDa; Fig. 6, lane 2), again consistent with the results reported by Le Fourn *et al.* (20).

To characterize the N-glycosylation process more precisely and to confirm immunofluorescence and flow cytometry results showing that TPOΔpro is transported to the cell surface, we isolated the intracellular and surface fraction of CHO cell proteins by the cell surface biotinylation technique. In this method, a membrane-impermeable reagent labeled with a biotin moiety forms a stable covalent linkage with amino groups of lysine residues that are exposed on the cell surface and are freely accessible to solvent. Subsequently, the intracellular and surface fractions were subjected to deglycosylation with Endo H or PNGase F (Fig. 7). Whereas PNGase F removes all N-linked oligosaccharides (high mannose- and complex-type structures), Endo H digests only mannose-type residues. Newly synthesized polypeptides first acquire high mannose carbohydrates, which are then modified (trimmed and remodeled) by a variety of transferases and glycosidases to complex oligosaccharides during passage through the Golgi apparatus. Therefore, we reasoned that using Endo H digestion to measure the amount of mannose and/or complex oligosaccharide attached to TPO would indicate if protein secretion occurs via the Golgi complex (43).

We detected TPO-specific bands in the intracellular and surface protein fractions, indicating that truncated TPO is transported to the cell membrane (Fig. 7, lanes 1 and 4), consistent with the data obtained by immunofluorescence and flow cytometry (Figs. 2 and 3). Surprisingly, the surface-presented TPOΔpro appeared as a distinct single band (Fig. 7, lane 1), while intracellular TPOΔpro migrated on the SDS-PAGE gel as a double band (Fig. 7, lane 4). After PNGase F digestion, the intracellular and surface fractions of TPOΔpro yielded a single band (Fig. 7, lanes 3 and 6). Endo H treatment of the intracellular fraction resulted in partial digestion of TPOΔpro (Fig. 7, lane 5), whereas the surface fraction was Endo H resistant (Fig. 7, lane 2). In conclusion, it appears that propeptide-deprived TPO, similarly to TPOwt, is transported to the cell surface by the secretory pathway mediated by the Golgi complex. The TPOΔpro propeptide bears high-mannose oligosaccharides that are transformed into a complex-type structure; therefore, all the TPOΔpro molecules detected at the cell surface are Endo H resistant. For comparison, part of the TPOwt molecules detected at the cell surface is still Endo H sensitive (20,22). These differences between TPOΔpro and TPOwt maturation will be discussed later.

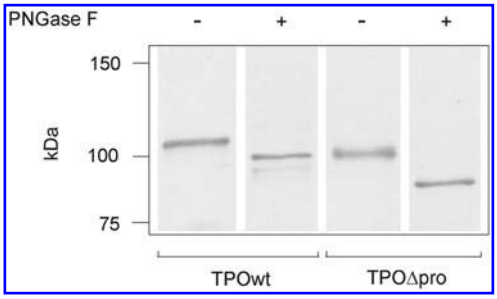

FIG. 6. Deglycosylation of TPOwt and TPOΔpro expressed in CHO cells. After digestion with PNGase F, total cell lysates were subjected to 8% SDS-PAGE, followed by Western blotting, and probing with anti-TPO mAb A4. Controls were done under the same conditions as the corresponding assay, except that enzyme was omitted. One representative immunoblot from independent experiments ($n \geq 3$) is shown.

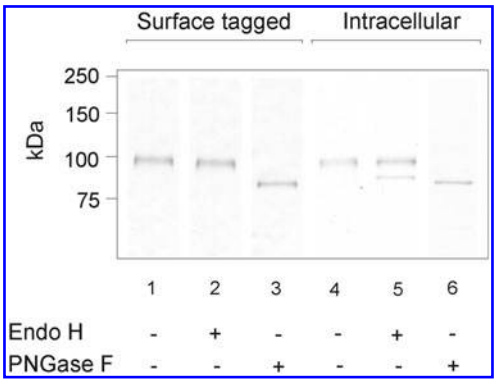

FIG. 7. Deglycosylation of TPOΔpro expressed in CHO cells present at the cell surface or in the intramolecular compartments with Endo H and PNGase F. After cell surface biotinylation and extraction, isolated proteins were digested with appropriate deglycosylation enzyme. Controls were done under the same conditions as the corresponding assay, except that enzymes were omitted. Samples were then subjected to SDS-PAGE, followed by Western blotting, and probing with anti-TPO mAb A4. One representative immunoblot from independent experiments ($n \geq 3$) is shown.

Molecular modeling and sequence analysis of TPOΔpro

The crystal structure of a mammalian thyroid peroxidase has not yet been determined. However, human TPO shares considerable sequence similarity with related human peroxidases of known three-dimensional structure (Supplementary Fig. S1; Supplementary Data are available online at www.liebertpub.com/thy). Alignment with the human sequences of eosinophil peroxidase, LPO, and MPO shows high similarity within the MPO-like domain, as well as the predicted signal peptide. However, while all sequences contain an N-terminal propeptide, there is virtually no detectable similarity in this region (Supplementary Fig. S1). It is interesting that TPO is unique in the animal heme-dependent peroxidase family in that it also contains two C-terminal domains, the CCP-like and the EGF-like domain (Supplementary Fig. S1).

The high sequence similarity of TPO with MPO-like domains with known crystal structures allowed us to build a homology model for the MPO-MPO domain dimer of TPOΔpro (Fig. 8). There are several reports of modeling, including from the authors (8,9) and from other laboratories (12–14). We

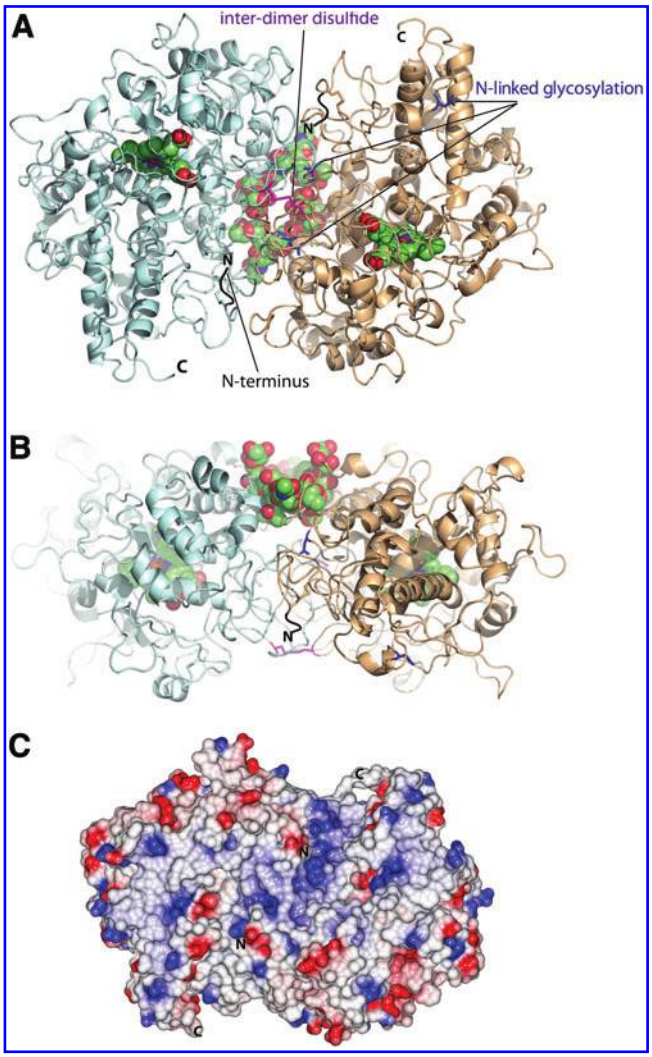

FIG. 8. Model of the myeloperoxidase (MPO)-like domain dimer of TPO. **(A, B)** Orthogonal views showing the dimer represented as cartoon with monomers colored differently. Heme groups buried in the core of each monomer are shown as space-filling atoms. Putative glycosylation sites are indicated by blue sticks and labeled, and the N-linked carbohydrate chains are also shown in space filling representation, making contact with each other at the edge of the dimer interface. The interdimer disulfide bridge is indicated in magenta. **(C)** Electrostatic potential surface of the TPO dimer model in same orientation as **(A)**. N- and C-termini are labeled; negative = red; positive = blue. Color images available online at www.liebertpub.com/thy

have exploited more recent high-resolution protein structures of homologues of the peroxidase family members and up-to-date molecular simulation methods in order to explore in more detail the structural and dynamic properties of the TPO dimer, and specifically the potential impact of propeptide removal and location of glycosylation sites. Our model has several important features. All three of the predicted asparagine-linked glycosylation sites (predicted using the NetNGlyc server; http://www.cbs.dtu.dk/services/NetNGlyc) map to the MPO-like domain, with one of them located at the dimer interface, mapping almost exactly to the location of the bound sugar moiety observed in the crystal structure of human MPO (incorporated in the TPO model; Fig. 8A). It is likely that the N-linked carbohydrate chain, consisting of $(GlcNac)_2$-$(Man)_3$ structure with a fucose 1–6 linked to the first GlcNac, makes stabilizing interactions with each MPO-like domain of TPO at the dimer interface in an analogous fashion to human MPO. Monomers are covalently linked by a disulfide bond that is conserved in members of the human peroxidases that adopt the MPO-like fold (Fig. 8), despite TPO, along with human MPO being the only members of the animal peroxidase family to exist as a functional dimer.

The structure of the N-terminal propeptide cannot be modeled with any confidence; except for the signal peptide region, it shares almost no sequence similarity with other human peroxidases (Supplementary Fig. S1). Interestingly, the propeptides of TPO, MPO, eosinophil peroxidase, and LPO are almost exactly the same length, with very few insertions or deletions. Despite the low similarity, there are nevertheless a few conserved residues, suggesting a very distant common ancestor; the extreme divergence in sequence is consistent with the lack of a structure-dependent functional role, which accords with our findings. Furthermore, the similar lengths of the propeptides also argue against a role in any interaction with the CCP- or EGF-like domains, since these domains are present uniquely in TPO. The TPO propeptide is moderately conserved among mammalian TPO enzymes (Supplementary Fig. S2), suggesting a rather limited role in folding and activity, also consistent with our findings. Our model predicts that the propeptide is most likely solvent exposed (Fig. 8); however, its likely location and mode of interaction with the dimer, if any, cannot be predicted with any confidence. Although it shares no sequence similarity with any known structure, it is not predicted to be disordered according to DisEMBL (44) and is predicted to be mainly helical according to PsiPred (45). The molecular surface of our TPOΔpro dimer model in the vicinity of where the propeptide would most likely reside is irregular, deeply pitted, and hydrophilic, with clusters of positively charged regions and smaller negatively charged patches (Fig. 8C). Given that the propeptide sequence is predicted to be positively charged at neutral pH (predicted pI = 10.2, containing 16 positively charged and 9 negatively charged residues), its interaction with the positively charged surface near the TPO-TPO dimer interface is probably relatively weak. This is again consistent with our findings.

Simulation of the model for 300 nanoseconds revealed overall moderate flexibility, although the dimer interface and the N-terminal regions were less flexible (Supplementary Video S1). The conserved disulfide bonds at the dimer interface and the intradomain bridge immediately after the propeptide are likely explanations for the observed rigidity in these regions. The flexibility elsewhere may be important in any structural rearrangements necessary to accommodate a propeptide.

Discussion

Newly synthesized TPO undergoes a number of post-translational modifications that result in a glycosylated, enzymatically active dimer located at the apical membrane of human thyrocytes. Moreover, during maturation, the propeptide region is proteolytically removed. In the present work for ongoing crystallization studies, we focused on the role of the propeptide TPO in expression, posttranslational modifications, and intracellular trafficking in CHO cells.

We report that propeptide-deleted TPO (TPOΔpro, lacking Pro21–Lys108) is expressed in CHO cells at a comparable level to TPOwt (depending on the method used for TPO expression determination). Importantly, TPOΔpro is transported to the cell surface and effectively recognized by antibodies with binding specificity for the two key TPO conformational determinants, IDR-A and IDR-B. Fayadat *et al.* (46) showed that correct TPO protein folding is a critical event in its biosynthesis and secretion. Only properly folded molecules are delivered to the cell membrane, while unfolded or partially unfolded/misfolded proteins are degraded by the proteasome or other proteases, respectively (46). More recently it was shown that nonproteosomal TPO degradation is mediated by plasminogen-like protease (47). Therefore, our findings that TPOΔpro is effectively transported to the cell surface where it reacts with conformation-dependent antibodies suggests that the presence of the propeptide is not necessary for proper folding of TPO. These findings contrast the results of Le Fourn *et al.* (20). Using metabolic labeling and cell surface protein biotinylation, they reported total inhibition of TPO transport to the cell membrane in CHO cells stably transfected with *TPOΔpro* cDNA.

Other studies of the role of the N-terminal propeptide in the folding of mammalian peroxidases are not unambiguously consistent with our findings. The best characterized member of this family is human MPO. Wild-type MPO is targeted for storage in granules by a regulated pathway, or secreted outside the cell by a constitutive pathway (43). Detailed studies on the role of the propeptide in maturation and sorting of MPO in myeloid 32D cell line revealed that MPOΔpro was effectively transported to the culture medium by the secretory pathway, but the intracellular trafficking to the storage granules was completely blocked (48). Therefore, the propeptide is likely to have an important role in the proper cellular sorting of MPO. In comparison, TPO targeting is less complicated since the protein only needs to be targeted to the cell surface. It has been shown that an MPO-TPO chimera, in which the amino terminus (residues 1–166) of full-length TPO was replaced with the homologous MPO propeptide (residues 1–121), was delivered to the cell surface of CHO cell, as determined by flow cytometry (18). This implies that the propeptide may not be required for the transportation of TPO and MPO to the cell membrane and outside the cell, respectively.

However, in a more recent article, it was shown that MPOΔpro is probably misfolded (49). An MPO mutant lacking the propeptide, stably expressed in K562 cells (a human hematopoietic cell line), failed to exit from the endoplasmic reticulum (49). In addition to MPO-TPO chimera proteins mentioned above, the fate of other fusion proteins tagged with the MPO propeptide and subsequently expressed in myeloid and nonmyeloid cell lines have been studied (49,50). In nonmyeloid cell lines (CHO cells and BHK cells), the propeptide directs lysozyme partly to an intracellular compartment and partly to the culture medium (50); however, in myeloid cell lines (32D, K562, and PLB-985), the presence of the propeptide was not sufficient to direct reporter proteins (soluble tumor necrosis factor-α receptor, green fluorescein protein, and α1-microglobulin) to the correct intracellular destination as in the case of wild-type MPO (49). It is possible that the propeptide alone is not sufficient to direct MPO to its proper intracellular destination in myeloid cells that normally process endogenously expressed MPO. It may be assumed that the propeptide of MPO interact via intramolecular interactions that are not reconstructed in the fusion proteins (49,50). Also, whereas TPO and MPO are dimers, other peroxidases are active in the monomeric form, and thus the interactions with the propeptide are likely to be different. The role of propeptide in the monomeric LPO in maturation and trafficking is poorly understood. It has been reported that LPOΔpro expressed in baculovirus-insect cells is secreted to the culture medium (as in wild-type LPO) in an enzymatically active form (51).

A possible explanation for the proper folding and sorting of TPOΔpro in comparison with MPOΔpro and LPOΔpro may lie in the unique domain architecture of TPO. In contrast to all other peroxidases, TPO contains C-terminal CCP-like and EGF-like domains, in addition to a membrane-anchoring segment. It is possible that these domains, which adopt compact, stable structures, interact favorably with the MPO-like domain of TPO, effectively stabilizing the TPO dimer such that its reliance on a propeptide for correct folding and assembly is lessened. Furthermore, subsequent anchoring to the membrane would be expected to add further stability to the folded dimer.

In the present study, we also focused on the impact of propeptide deletion on the asparagine-glycosylation process. Asparagine-linked glycosylation is known to favorably enhance the folding and sorting of nascent protein in several ways. Attached oligosaccharide moieties are recognized by lectin-like molecular chaperones such as calnexin and calreticulin, promoting correct protein folding. Furthermore, N-glycans stabilize the structure of proteins and play a role in their quality control and adequate sorting (52,53). Here we provide evidence that TPOΔpro is N-glycosylated and possesses high-mannose N-linked oligosaccharides that are subsequently completely processed into complex carbohydrate side chain moieties. MPOΔpro secreted to the culture medium also contains only complex-type N-linked moieties (48). This observation may support our conclusion that TPOΔpro, similarly to previously reported MPOΔpro (48), is transported from the endoplasmic reticulum to the cell surface through the secretory pathway. During transit, TPOΔpro and MPOΔpro are transferred to the Golgi apparatus where they acquire complex oligosaccharides. However, we cannot exclude that the N-glycosylation process of membrane-anchored TPOΔpro and secreted MPOΔpro is different to some extent. This is consistent with the observation that the subcellular fraction of MPOΔpro is susceptible to Endo H (48), while TPOΔpro detected inside the cell is only partly Endo H resistant. It is tempting to speculate that this discrepancy may be assigned to the different cell lines used for expression of truncated TPO (CHO cell line) and truncated MPO (32D cell line).

Our results revealed that TPOΔpro is enzymatically active and forms dimers. It has already been demonstrated that the attachment of heme residues to the TPO molecule is essential for delivery of TPO to the cell surface (54). The MPO molecule, as well as all other members of the mammalian peroxidase family, contains heme as a prosthetic group (43). Heme is incorporated into MPO before its exit from the endoplasmic reticulum and is required for proper folding (55). Interestingly, human MPOΔpro is enzymatically active (with some minor reduction in efficiency of heme incorporation in comparison with wild-type MPO) when expressed in 32D cells (48); however, the same construct expressed in K562 cells

lacked heme (49). Importantly, human LPOΔpro demonstrated similar enzyme activity compared with the activity of recombinant wild-type LPO and bovine LPO (51). Also, inhibition of propeptide cleavage in TPOwt expressed in CHO cells increased its enzymatic activity protein, implying that enzyme activity is not hindered by the presence of the propeptide (20). Taken together, the evidence suggests that the propeptide has no observable impact on enzymatic activity of TPO (neither negative nor positive), and this may also apply to other mammalian peroxidases, at least for MPO and LPO. In this study we have shown for the first time that TPOΔpro forms enzymatically active dimers, supporting our hypothesis that truncated TPO matures properly in CHO cells. In addition to TPO, MPO is the only other mammalian peroxidase that forms dimers that are necessary for targeting to the granules—all other secreted members of the family exist as monomers (43).

It has been suggested that the propeptide of TPO functions as an intramolecular chaperone (20). Such intramolecular chaperones are generally encoded as an N-terminal or a C-terminal extension and do not contribute to the protein function, but they are critical for proper folding. The intramolecular chaperones are removed from the proteins when the folding process is completed (56). It is often observed that the intramolecular chaperone and the associated protein need not be covalently linked for correct chaperone function (57). Co-expression in *trans* of TPO propeptide and TPOΔpro in CHO cells did not restore the proper folding of truncated TPO (20). A similar conclusion was drawn by Bülow *et al.* (49) with reference to MPO.

It remains unclear why our results presented here contrast with observations indicating an important role of the propeptide in TPO folding and sorting (20). There are several differences between this and the previous study that may contribute to the discrepancies. Our TPOΔpro construct contained a 20-residue signal peptide compared to 14 residues in the study by Le Fourn *et al*. (20). Importantly, Le Fourn *et al.* (20) also examined the effect of using a slightly longer leader sequence (residues 1–26); however, they did not observe any improvement in TPOΔpro expression and maturation. Additionally, in contrast to the mouse anti-TPO antibody that binds to both partially and completely folded TPO used by Le Fourn *et al.* (20), we used a different and wider panel of human anti-TPO mAbs that have been shown to be specific to conformational epitopes on properly folded TPO (6,8,11).

In summary, we present for the first time an in-depth investigation into the role of the propeptide in the folding, sorting, and function of recombinant human TPO. We provide novel data suggesting that truncated TPO is effectively expressed, transported, and matured in CHO cells. In addition we have performed modeling that allows us to rationalize the role of glycosylation and the propeptide on a structural basis. Therefore, we suggest that it is highly likely that the propeptide of TPO does not function as an intramolecular chaperone. Nevertheless, it is unlikely that a propeptide that constitutes approximately 10% of the whole TPO molecule does not play some role in TPO structure and function. It cannot be excluded that the full-length protein possesses additional, important properties compared to the truncated version. For example, the propeptide may play a role in accelerating folding, as observed for subtilisin (58), or making key interactions during the folding pathway that reduce the accumulation of off-pathway folding intermediates and aggregates.

Acknowledgments

We acknowledge Emeritus Professor A. Gardas (Department of Biochemistry and Molecular Biology, Medical Center of Postgraduate Education) for helpful discussions. We thank Wanda Krasuska (Department of Biochemistry and Molecular Biology, Medical Center of Postgraduate Education) for technical assistance. This work was supported by grants from the Medical Center of Postgraduate Education No. 501-1-1-25-04/09 and 501-1-25-01-12. A.M.B. is supported by an National Health and Medical Research Committee Senior Research Fellowship.

Disclosure Statement

The authors report no conflicts of interest. The authors alone are responsible for the content and writing of the paper.

References

1. Kopp P 2012 Thyroid hormone synthesis. In: Braverman LE, Cooper D (eds) Werner and Ingbar's the Thyroid: A Fundamental and Clinical Text. Tenth edition. Lippincott Williams & Wilkins, Philadelphia, pp 48–74.
2. Banga JP 1998 Developments in our understanding of the structure of thyroid peroxidase and the relevance of these findings to autoimmunity. Curr Opin Endocrinol Diabetes **5:**275–281.
3. Gora M, Dubska M, Jastrzebska-Bohaterewicz E, Gardas A 2006 Profile of autoantibodies to the two immunodominant regions of thyroid peroxidase in autoimmunity. In: Wiersinga WM, Drexhage HA, Weetman AP, Butz S (eds) The Thyroid and Autoimmunity. Georg Thieme Verlag, New York, pp 110–117.
4. McLachlan SM, Rapoport B 2007 Thyroid peroxidase as an autoantigen. Thyroid **17:**939–948.
5. Ruf J, Toubert ME, Czarnocka B, Durand-Gorde JM, Ferrand M, Carayon P 1989 Relationship between immunological structure and biochemical properties of human thyroid peroxidase. Endocrinology **125:**1211–1218.
6. Czarnocka B, Janota-Bzowski M, McIntosh RS, Asghar MS, Watson PF, Kemp EH, Carayon P, Weetman AP 1997 Immunoglobulin G kappa antithyroid peroxidase antibodies in Hashimoto's thyroiditis: epitope-mapping analysis. J Clin Endocrinol Metab **82:**2639–2644.
7. Chazenbalk GD, Portolano S, Russo D, Hutchison JS, Rapoport B, McLachlan S 1993 Human organ-specific autoimmune disease. Molecular cloning and expression of an autoantibody gene repertoire for a major autoantigen reveals an antigenic immunodominant region and restricted immunoglobulin gene usage in the target organ. J Clin Invest **92:**62–74.
8. Dubska M, Banga JP, Plochocka D, Hoser G, Kemp EH, Sutton BJ, Gardas A, Gora M 2006 Structural insights into autoreactive determinants in thyroid peroxidase composed of discontinuous and multiple key contact amino acid residues contributing to epitopes recognized by patients' autoantibodies. Endocrinology **147:**5995–6003.
9. Hobby P, Gardas A, Radomski R, McGregor AM, Banga JP, Sutton BJ 2000 Identification of an immunodominant region recognized by human autoantibodies in a three-dimensional model of thyroid peroxidase. Endocrinology **141:**2018–2026.
10. Gora M, Gardas A, Wiktorowicz W, Hobby P, Watson PF, Weetman AP, Sutton BJ, Banga JP 2004 Evaluation of conformational epitopes on thyroid peroxidase by antipeptide

antibody binding and mutagenesis. Clin Exp Immunol **136:**137–144.
11. Gora M, Gardas A, Watson PF, Hobby P, Weetman AP, Sutton BJ, Banga JP 2004 Key residues contributing to dominant conformational autoantigenic epitopes on thyroid peroxidase identified by mutagenesis. Biochem Biophys Res Commun **320:**795–801.
12. Bresson D, Cerutti M, Devauchelle G, Pugnière M, Roquet F, Bes C, Bossard C, Chardès T, Péraldi-Roux S 2003 Localization of the discontinuous immunodominant region recognized by human anti-thyroperoxidase autoantibodies in autoimmune thyroid diseases. J Biol Chem **278:**9560–9569.
13. Bresson D, Pugnière M, Roquet F, Rebuffat SA, N-Guyen B, Cerutti M, Guo J, McLachlan SM, Rapoport B, Estienne V, Ruf J, Chardès T, Péraldi-Roux S 2004 Directed mutagenesis in region 713–720 of human thyroperoxidase assigns 713KFPED717 residues as being involved in the B domain of the discontinuous immunodominant region recognized by human autoantibodies. J Biol Chem **279:**39058–39067.
14. Nishikawa T, Rapoport B, McLachlan SM 1996 The quest for the autoantibody immunodominant region on thyroid peroxidase: guided mutagenesis based on a hypothetical three-dimensional model. Endocrinology **137:**1000–1006.
15. Guo J, Yan XM, McLachlan SM, Rapoport B 2001 Search for the autoantibody immunodominant region on thyroid peroxidase: epitopic footprinting with a human monoclonal autoantibody locates a facet on the native antigen containing a highly conformational epitope. J Immunol **166:**1327–1333.
16. Nishikawa T, Rapoport B, McLachlan SM 1994 Exclusion of two major areas on thyroid peroxidase from the immunodominant region containing the conformational epitopes recognized by human autoantibodies. J Clin Endocrinol Metab **79:**1648–1654.
17. Guo J, McLachlan SM, Rapoport B 2002 Localization of the thyroid peroxidase autoantibody immunodominant region to a junctional region containing portions of the domains homologous to complement control protein and myeloperoxidase. J Biol Chem **277:**40189–40195.
18. Nishikawa T, Nagayama Y, Seto P, Rapoport B 1993 Human thyroid peroxidase-myeloperoxidase chimeric molecules: tools for the study of antigen recognition by thyroid peroxidase autoantibodies. Endocrinology **133:**2496–2501.
19. Kimura S, Kotani T, McBride OW, Umeki K, Hirai K, Nakayama T, Ohtaki S 1987 Human thyroid peroxidase: complete cDNA and protein sequence, chromosome mapping, and identification of two alternately spliced mRNAs. Proc Natl Acad Sci USA **84:**5555–5559.
20. Le Fourn V, Ferrand M, Franc JL 2005 Endoproteolytic cleavage of human thyroperoxidase: role of the propeptide in the protein folding process. J Biol Chem **280:**4568–4577.
21. Ruf J, Carayon P 2006 Structural and functional aspects of thyroid peroxidase. Arch Biochem Biophys **445:**269–277.
22. Fayadat L, Niccoli-Sire P, Lanet J, Franc JL 1998 Human thyroperoxidase is largely retained and rapidly degraded in the endoplasmic reticulum. Its N-glycans are required for folding and intracellular trafficking. Endocrinology **139:**4277–4285.
23. Kuliawat R, Ramos-Castañeda J, Liu Y, Arvan P 2005 Intracellular trafficking of thyroid peroxidase to the cell surface. J Biol Chem **280:**27713–27718.
24. Zhang X, Arvan P 2000 Cell type-dependent differences in thyroid peroxidase cell surface expression. J Biol Chem **275:**31946–31953.
25. Fayadat L, Siffroi-Fernandez S, Lanet J, Franc JL 2000 Calnexin and calreticulin binding to human thyroperoxidase is required for its first folding step(s) but is not sufficient to promote efficient cell surface expression. Endocrinology **141:**959–966.
26. Le Fourn V, Siffroi-Fernandez S, Ferrand M, Franc JL 2006 Competition between calnexin and BiP in the endoplasmic reticulum can lead to the folding or degradation of human thyroperoxidase. Biochemistry **45:**7380–7388.
27. Gardas A, Lewartowska A, Sutton BJ, Pasieka Z, McGregor AM, Banga JP 1997 Human thyroid peroxidase (TPO) isoforms, TPO-1 and TPO-2: analysis of protein expression in Graves' thyroid tissue. J Clin Endocrinol Metab **82:**3752–3757.
28. Ferrand M, Le Fourn V, Franc JL 2003 Increasing diversity of human thyroperoxidase generated by alternative splicing. Characterized by molecular cloning of new transcripts with single- and multispliced mRNAs. J Biol Chem **278:**3793–3800.
29. McIntosh RS, Asghar MS, Kemp EH, Watson PF, Gardas A, Banga JP, Weetman AP 1997 Analysis of immunoglobulin G kappa antithyroid peroxidase antibodies from different tissues in Hashimoto's thyroiditis. J Clin Endocrinol Metab **82:**3818–3825.
30. Ewins DL, Barnett PS, Tomlinson RW, McGregor AM, Banga JP 1992 Mapping epitope specificities of monoclonal antibodies to thyroid peroxidase using recombinant antigen preparations. Autoimmunity **11:**141–149.
31. Ho SN, Hunt HD, Horton RM, Pullen JK, Pease LR 1989 Site-directed mutagenesis by overlap extension using the polymerase chain reaction. Gene **77:**51–59.
32. Fortunato RS, Lima de Souza EC, Ameziane-el Hassani R, Boufraqech M, Weyemi U, Talbot M, Lagente-Chevallier O, de Carvalho DP, Bidart JM, Schlumberger M, Dupuy C 2010 Functional consequences of dual oxidase-thyroperoxidase interaction at the plasma membrane. J Clin Endocrinol Metab **95:**5403–5411.
33. Larkin MA, Blackshields G, Brown NP, Chenna R, McGettigan PA, McWilliam H, Valentin F, Wallace IM, Wilm A, Lopez R, Thompson JD, Gibson TJ, Higgins DG 2007 Clustal W and Clustal X version 2.0. Bioinformatics **23:**2947–2948.
34. Eswar N, Webb B, Marti-Renom MA, Madhusudhan MS, Eramian D, Shen MY, Pieper U, Sali A 2007 Comparative protein structure modeling using MODELLER. Curr Protoc Protein Sci **Chapter 2:**Unit 2.9.
35. Hess B, Kutzner C, van der Spoel D, Lindahl E 2008 GROMACS 4: Algorithms for highly efficient, load-balanced, and scalable molecular simulation. Journal of Chemical Theory and Computation **4:**435–447.
36. Oostenbrink C, Villa A, Mark AE, van Gunsteren WF 2004 A biomolecular force field based on the free enthalpy of hydration and solvation. J Comput Chem **25:**1656–1676.
37. Berendsen HJC, Postma JPM, van Gunsteren WF 1981 Interaction models for water in relation to protein hydration. In: Pullman B (ed) Intermolecular Forces. Reidel, Dordrecht, The Netherlands, pp 331–342.
38. Berendsen HJC, Postma JPM, Vangunsteren WF, Dinola A, Haak JR 1984 Molecular-dynamics with coupling to an external bath. J Chem Phys **81:**3684–3690.
39. Hess B, Bekker H, Berendsen HJC, Fraaije JGEM 1997 LINCS: A linear constraint solver for molecular simulations. J Comput Chem **18:**1463–1472.
40. Miyamoto S, Kollman PA 1992 Settle—an analytical version of the SHAKE and RATTLE algorithm for rigid water models. J Comput Chem **13:**952–962.

41. Tironi IG, Sperb R, Smith PE, Vangunsteren WF 1995 A generalized reaction field method for molecular-dynamics simulations. J Chem Phys **102:**5451–5459.
42. Heinz TN, van Gunsteren WF, Hunenberger PH 2001 Comparison of four methods to compute the dielectric permittivity of liquids from molecular dynamics simulations. J Chem Phys **115:**1125–1136.
43. Hansson M, Olsson I, Nauseef WM 2006 Biosynthesis, processing, and sorting of human myeloperoxidase. Arch Biochem Biophys **445:**214–224.
44. Linding R, Jensen LJ, Diella F, Bork P, Gibson TJ, Russell RB 2003 Protein disorder prediction: implications for structural proteomics. Structure **11:**1453–1459.
45. Buchan DW, Ward SM, Lobley AE, Nugent TC, Bryson K, Jones DT 2010 Protein annotation and modelling servers at University College London. Nucleic Acids Res **38:**W563–W568.
46. Fayadat L, Siffroi-Fernandez S, Lanet J, Franc JL 2000 Degradation of human thyroperoxidase in the endoplasmic reticulum involves two different pathways depending on the folding state of the protein. J Biol Chem **275:**15948–15954.
47. Giraud A, Lejeune PJ, Barbaria J, Mallet B 2007 A plasminogen-like protease in thyroid rough microsomes degrades thyroperoxidase and thyroglobulin. Endocrinology **148:**2886–2893.
48. Andersson E, Hellman L, Gullberg U, Olsson I 1998 The role of the propeptide for processing and sorting of human myeloperoxidase. J Biol Chem **273:**4747–4753.
49. Bülow E, Nauseef WM, Goedken M, McCormick S, Calafat J, Gullberg U, Olsson I 2002 Sorting for storage in myeloid cells of nonmyeloid proteins and chimeras with the propeptide of myeloperoxidase precursor. J Leukoc Biol **71:**279–288.
50. Bening U, Castino R, Harth N, Isidoro C, Hasilik A 1998 Lysosomal segregation of a mannose-rich glycoprotein imparted by the prosequence of myeloperoxidase. J Cell Biochem **71:**158–168.
51. Fragoso MA, Torbati A, Fregien N, Conner GE 2009 Molecular heterogeneity and alternative splicing of human lactoperoxidase. Arch Biochem Biophys **482:**52–57.
52. Helenius A, Aebi M 2004 Roles of N-linked glycans in the endoplasmic reticulum. Annu Rev Biochem **73:**1019–1049.
53. Ungar D 2009 Golgi linked protein glycosylation and associated diseases. Semin Cell Dev Biol **20:**762–769.
54. Fayadat L, Niccoli-Sire P, Lanet J, Franc JL 1999 Role of heme in intracellular trafficking of thyroperoxidase and involvement of H2O2 generated at the apical surface of thyroid cells in autocatalytic covalent heme binding. J Biol Chem **274:**10533–10538.
55. Nauseef WM, McCormick S, Yi H 1992 Roles of heme insertion and the mannose-6-phosphate receptor in processing of the human myeloid lysosomal enzyme, myeloperoxidase. Blood **80:**2622–2633.
56. Chen YJ, Inouye M 2008 The intramolecular chaperone-mediated protein folding. Curr Opin Struct Biol **18:**765–770.
57. Shinde U, Inouye M 2000 Intramolecular chaperones: polypeptide extensions that modulate protein folding. Semin Cell Dev Biol **11:**35–44.
58. Almog O, Gallagher T, Tordova M, Hoskins J, Bryan P, Gilliland GL 1998 Crystal structure of calcium-independent subtilisin BPN′ with restored thermal stability folded without the prodomain. Proteins **31:**21–32.

Address correspondence to:
Marlena Godlewska, PhD
Medical Center of Postgraduate Education
Department of Biochemistry and Molecular Biology
Marymoncka 99/103
01-813 Warsaw
Poland

E-mail: marlena@cmkp.edu.pl